Low-Temperature Experimental and Theoretical Rate Constants for the O(1 D) + H 2 Reaction

Kevin Hickson, Yury V Suleimanov

▶ **To cite this version:**

Kevin Hickson, Yury V Suleimanov. Low-Temperature Experimental and Theoretical Rate Constants for the O(1 D) + H 2 Reaction. Journal of Physical Chemistry A, 2017, 121 (9), pp.1916-1923. ⟨10.1021/acs.jpca.7b00722⟩. ⟨hal-03105472⟩

HAL Id: hal-03105472

https://hal.science/hal-03105472v1

Submitted on 11 Jan 2021

HAL is a multi-disciplinary open access archive for the deposit and dissemination of scientific research documents, whether they are published or not. The documents may come from teaching and research institutions in France or abroad, or from public or private research centers.

L'archive ouverte pluridisciplinaire **HAL**, est destinée au dépôt et à la diffusion de documents scientifiques de niveau recherche, publiés ou non, émanant des établissements d'enseignement et de recherche français ou étrangers, des laboratoires publics ou privés.

HAL Authorization

Low Temperature Experimental and Theoretical Rate Constants for the $O(^1D) + H_2$ Reaction

Kevin M. Hickson[*,†,‡] *and Yury V. Suleimanov*[*,∥,^]

[†] Université de Bordeaux, Institut des Sciences Moléculaires, F-33400 Talence, France

[‡] CNRS, Institut des Sciences Moléculaires, F-33400 Talence, France

[∥] Computation-based Science and Technology Research Center, Cyprus Institute, 20 Kavafi Str., Nicosia 2121, Cyprus

^ Department of Chemical Engineering, Massachusetts Institute of Technology, 77 Massachusetts Ave., Cambridge, Massachusetts 02139, United States

AUTHOR INFORMATION

Corresponding Authors

km.hickson@ism.u-bordeaux1.fr, y.suleymanov@cyi.ac.cy

Abstract

In the present joint experimental and theoretical study, we report thermal rate constants for the $O(^1D)$ + H_2 reaction within the 50-300 K temperature range. Experimental kinetics measurements were performed using a continuous supersonic flow reactor coupled with pulsed laser photolysis for $O(^1D)$ production and pulsed laser induced fluorescence in the vacuum ultraviolet wavelength range (VUV LIF) for $O(^1D)$ detection. Theoretical rate constants were obtained using the ring polymer molecular dynamics (RPMD) approach over the two lowest potential energy surfaces $1^1A'$ and $1^1A''$ which possess barrierless and thermally activated energy profiles, respectively. Both the experimental and theoretical rate constants exhibit a weak temperature dependence. The theoretical results show the dominant role of the $1^1A'$ ground state and that contribution of the $1^1A''$ excited state to the total thermal rate decreases dramatically at lower temperature. The agreement between the experimental and theoretical results is good, the discrepancy does not exceed 25 %. It is argued that these differences are likely to be due to non-adiabatic couplings between the $1^1A'$ and $2^1A'$ surfaces.

1 Introduction

The reactions of atomic oxygen in its first excited state, $O(^1D)$, play important roles in the chemistry of planetary atmospheres and in the interstellar medium. In the Earth's atmosphere the photodissociation of stratospheric O_3 leads to the production of $O(^1D)$ atoms with high quantum yields in the ultraviolet wavelength range.[1] Although the primary fate of $O(^1D)$ atoms formed in this way is quenching to the ground ^3P state through collisions with the primary atmospheric constituents N_2 and O_2,[2] a fraction of these $O(^1D)$ atoms react rapidly with trace atmospheric molecules. As the upper atmosphere is relatively dry, given that the tropopause acts as a cold trap for moist air rising from the troposphere, stratospheric OH radicals which participate in catalytic ozone destruction cycles are mostly formed by the reactions of $O(^1D)$ with CH_4[3] and with H_2,[4] present in the stratosphere with mixing ratios of 1.7×10^{-6} and 5×10^{-7} respectively. $O(^1D)$ atoms are also important in astrochemistry. The major constituent of the Martian atmosphere is carbon dioxide (95 %) which is readily photolysed below 205 nm to produce CO molecules and atomic oxygen. As the three body recombination reaction $CO + O + M \rightarrow CO_2 + M$ is slow,[5] it is expected that CO and O_2 should be present at high levels in the Martian atmosphere. Interestingly, CO and O_2 concentrations derived from observations[6, 7] are at least a factor 30 too low (more than 100 for CO), suggesting that other processes act to maintain CO_2 levels. The OH + CO reaction is one potentially important process in this respect and catalyzes the reconversion of CO to CO_2. OH radicals themselves are generated by water photolysis in the vacuum ultraviolet (VUV) range and also through the reactions of $O(^1D)$ atoms (produced by the photodissociation of CO_2 below 170 nm and through O_3 photolysis) with both H_2 and H_2O.

The kinetics of the $O(^1D) + H_2$ reaction have previously been investigated experimentally at both room temperature[8-13] and over a range of temperatures. [4, 14, 15] These studies have shown that the reaction is fast ($k_{O(1D)+H2} \geq 10^{-10}$ cm^3 s^{-1}) and displays only weak

variations of the rate constant as a function of temperature in the range 195 - 420 K.[4, 14, 15] There are also numerous studies of the dynamical aspects of the $O(^1D) + H_2$ reaction at both the experimental[16-21] and theoretical[17, 19-40] levels, employing a variety of theoretical techniques ranging from statistical theory, [26, 38, 39] quasi-classical trajectory (QCT) methods,[17, 19-23, 25, 27, 32] as well as approximate and detailed quantum mechanical (QM) calculations.[19, 20, 24, 29-31, 33-35, 37, 40] As an insertion type reaction which typically involve deep potential wells, the use of QM methods is computationally expensive given the need to treat large numbers of bound quantum states. Consequently, in recent years there has been a significant effort to develop novel theoretical strategies to treat such systems efficiently while simultaneously providing an accurate description of QM effects such as zero-point energy and tunneling. One method, namely ring polymer molecular dynamics (RPMD) rate theory has been demonstrated[41] to provide reliable estimates for insertion type chemical reactions[3, 36, 42-45] as well as for thermally activated chemical reactions[46-61] and even for reactions with more complex energy profiles.[62-64] In particular, RPMD rate constants calculated for a similar chemical reaction between $C(^1D)$ and H_2 at low temperatures (300-50 K) demonstrated excellent agreement with the measured ones.[43]

The interaction between $O(^1D)$ and $H_2(X^1\Sigma_g^+)$ gives rise to five singlet states. Two of these are strongly repulsive leaving three singlet states which might play a role in the reaction. The ground $1^1A'$ surface correlates adiabatically with $O(^1D)$ and $H_2(X^1\Sigma_g^+)$ reagents and ground state products $OH(X^2\Pi)$ and $H(^2S)$ in the absence of a barrier.[65, 66] This pathway is characterized by a deep potential well corresponding to a long-lived H_2O intermediate and is distinguishable in the experimental[17] and theoretical[24] results through a notable backward forward symmetry in the differential cross sections (DCSs) at low collision energy. Two other surfaces are also potentially involved in the $O(^1D) + H_2(X^1\Sigma_g^+)$ reaction. The first excited $1^1A''$ state also correlates adiabatically with ground state products $OH(X^2\Pi)$ and $H(^2S)$, although this surface

is characterized by the presence of an activation barrier (10 kJ mol^{-1}) and no potential well, where reaction occurs through an abstraction type mechanism. The contribution of this channel is expected to increase at higher energies and can be identified by the presence of an asymmetry in the experimental[17] and theoretical[37] DCSs. Finally, the $2^1A'$ surface correlates adiabatically with excited state $OH(A^2\Sigma^+)$ and $H(^2S)$ products. While this surface shares the same activation barrier as the $1^1A''$ state, the presence of a small potential well (lower in energy than the separated reagents) and a conical intersection to the ground $1^1A'$ surface might allow this state to contribute to the overall reactivity through a non-adiabatic pathway. This particular channel could play a role in the reaction dynamics at both high and low energies. At high energy, the activation barrier is easier to overcome in a similar manner to the $1^1A''$ state. At low energy, although passage over the barrier is now inhibited, reaction could still occur by tunneling. Moreover, as the weakly bound complex lifetime increases at low energy, the probability for non-adiabatic transitions to occur to the ground $1^1A'$ surface could be enhanced.

In order to evaluate the contribution of these excited states to the overall reactivity of the $O(^1D) + H_2$ system, it is important to study this process at even lower energies and/or temperatures where quantum effects are likely to be more pronounced. To address this issue, we undertook a joint experimental and theoretical investigation of the $O(^1D) + H_2$ reaction. On the experimental side, a continuous flow supersonic reactor was used to study the reaction over the 50-296 K range, employing pulsed laser photolysis and pulsed laser induced fluorescence as production and detection methods respectively to follow the $O(^1D)$ kinetics. On the theoretical side, the RPMD method was employed to study the dynamics of the title reaction over the ground $1^1A'$ and excited $1^1A''$ surfaces and to furnish rate constants in the same temperature range. The experimental and theoretical methods used in this work and the corresponding results are described in sections 2 and 3. A discussion of these results and our conclusions are presented in section 4.

2 Experimental Methods and Results

The measurements reported here were performed using a continuous flow supersonic reactor (also known as the CRESU technique - *Cinétique de Réaction en Ecoulement Supersonique Uniforme*) which has been described in detail in earlier work,[67] with other details relevant to the current investigation presented in later studies.[2, 3, 43, 44, 68] These experiments were conducted at specific low temperatures of 127 K, 75 K and 50 K through the use of three individual Laval nozzles. In addition, experiments at ambient temperature (296 K) were performed by removing the Laval nozzle and by reducing the flow velocity. The calculated flow characteristics (temperature, density, velocity and pressure) for these nozzles are presented in Table 1 of Grondin et al.[2] Only argon based nozzles were used in the present work as the nitrogen based ones resulted in the efficient removal of $O(^1D)$ atoms through quenching to the ground triplet state.[2]

$O(^1D)$ atoms were generated in-situ within the cold supersonic flow by the photolysis of ozone (O_3) at 266 nm with pulse energies around 20 mJ. The quantum yield for $O(^1D)$ formation at 266 nm is approximately 0.9.[1] O_3 itself was produced by the continuous ultraviolet (UV) irradiation of O_2 in a quartz cell by a high pressure mercury lamp as described in Grondin et al.[2] The UV photolysis of O_2 led to $O(^3P)$ formation which then recombined with non-dissociated O_2; a process whose yield was improved by the use of higher pressures (700 Torr). The contents of the cell (O_3/O_2) were mixed with the carrier gas Ar and reagent H_2 upstream of the Laval nozzle.

A direct detection method was employed in the present experiments. Tunable light around 115 nm was generated in a two-step process. Firstly, a pulsed narrow band dye laser operating around 690 nm was frequency doubled to produce 345 nm light. Residual radiation at 690 nm was eliminated before the UV beam was focused into a cell containing 100 Torr of xenon and

230 Torr of argon for phase matching purposes. The VUV light produced by frequency tripling in xenon was collimated by a magnesium fluoride lens at the exit of the cell. O(^{1}D) atoms were excited through the the 3s ^{1}D – 2p ^{1}D transition at 115.215 nm and the resonant vacuum ultraviolet laser induced fluorescence emission (VUV LIF) from unreacted O(^{1}D) atoms was detected using a solar blind photomultiplier tube (PMT). The PMT was isolated from the flow reactor by a Lithium Fluoride (LiF) window and the volume between the PMT and the window was evacuated to prevent atmospheric absorption of the emitted VUV light. A LiF lens within the evacuated region collected the VUV emission and focused it onto the PMT photocathode. A boxcar integration system was used for signal processing and acquisition.

VUV LIF signals were recorded as a function of time between the photolysis and probe lasers with the lasers and acquisition electronics being synchronized by a pulsed delay generator. During the kinetic measurements, each time point consisted of an average of 30 laser shots, with at least 70 time points recorded for each decay profile. The pretrigger baseline signal (containing scattered light contributions from the probe laser and any other spurious electronic noise), was established by firing the probe laser at several time intervals prior to the photolysis laser.

All of the gases used in these measurements (Ar 99.999%, H_2 99.999%, O_2 99.999%, Xe 99.998%) were flowed directly from cylinders without further purification. As calibrated mass flow controllers were employed to drive the gas flows, the excess reagent and carrier gas concentrations could be determined from the flow ratios and the calculated flow density.

To simplify the kinetic analysis, the pseudo-first-order approximation was applied by using a large excess of H_2 with respect to O(^{1}D). Consequently, the H_2 concentration was effectively constant for all of the individual measurements presented here. Under these conditions, the O(^{1}D) VUV LIF signal was seen to obey a first-order decay law of the type $I_t = I_0 \exp(-k't)$, where I_t and I_0 are the time dependent and initial signal intensities respectively, k' is the pseudo-

first-order rate constant for $O(^1D)$ loss and t is time. Typical reagent $O(^1D)$ decay profiles recorded at 50 K as a function of the delay between the photolysis and probe lasers are shown in Figure 1.

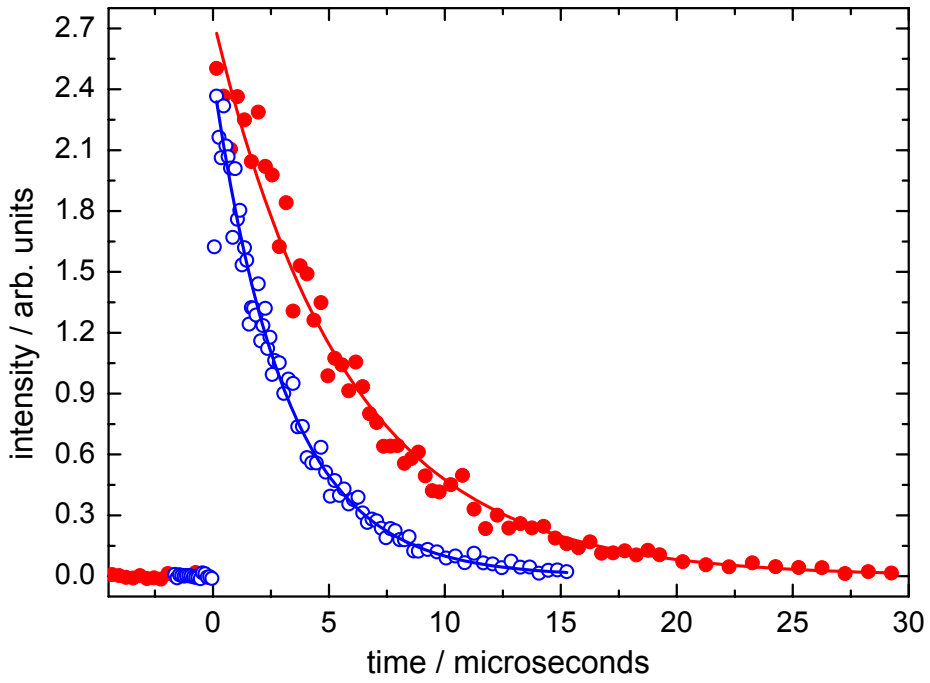

Figure 1 $O(^1D)$ atom decay curves recorded at 50 K. (blue open circles) $[H_2] = 1.1 \times 10^{15}$ cm^{-3}; (Red solid circles) in the absence of $[H_2]$ ($O(^1D)$ atoms decay rapidly through non-reactive quenching with the carrier gas Ar). Solid lines represent single exponential fits to the data of the form $I_t = I_0 \exp(-k't)$ (see text).

It can be seen from Figure 1 that even in the absence of H_2, $O(^1D)$ atoms decay rapidly with a pseudo-first-order loss rate of 1.8×10^5 s^{-1}. During these experiments, $O(^1D)$ atoms are potentially removed by several different non-reactive processes such as quenching by the carrier gas Ar, quenching by residual O_2 in the reactor and/or by diffusional loss. During our recent investigation of the $O(^1D) + N_2$ and O_2 quenching processes[2] we determined temperature

dependent rate constants for removal by both O_2 and Ar with values of 6.6×10^{-11} cm^3 s^{-1} and 6.8×10^{-13} cm^3 s^{-1} at 50 K respectively. In the present example, $[O_2] = 6.8 \times 10^{13}$ cm^{-3} and [Ar] $= 2.6 \times 10^{17}$ cm^{-3}; values which lead to $O(^1D)$ pseudo-first order loss rates of 4.5×10^3 s^{-1} and 1.8×10^5 s^{-1} respectively. Consequently, $O(^1D)$ losses in the absence of H_2 are almost entirely due to collisions with Ar, whereas other processes contribute at a negligible level.

Second-order rate constants were determined at any given temperature by plotting the measured pseudo-first-order rate constants against the corresponding H_2 concentration. The H_2 concentration was varied over a wide range of values to reduce the associated statistical uncertainties on the derived second-order rates with at least 40 individual measurements performed at every temperature. Exemplary second-order plots obtained at 296 K and at 50 K are displayed in Figure 2.

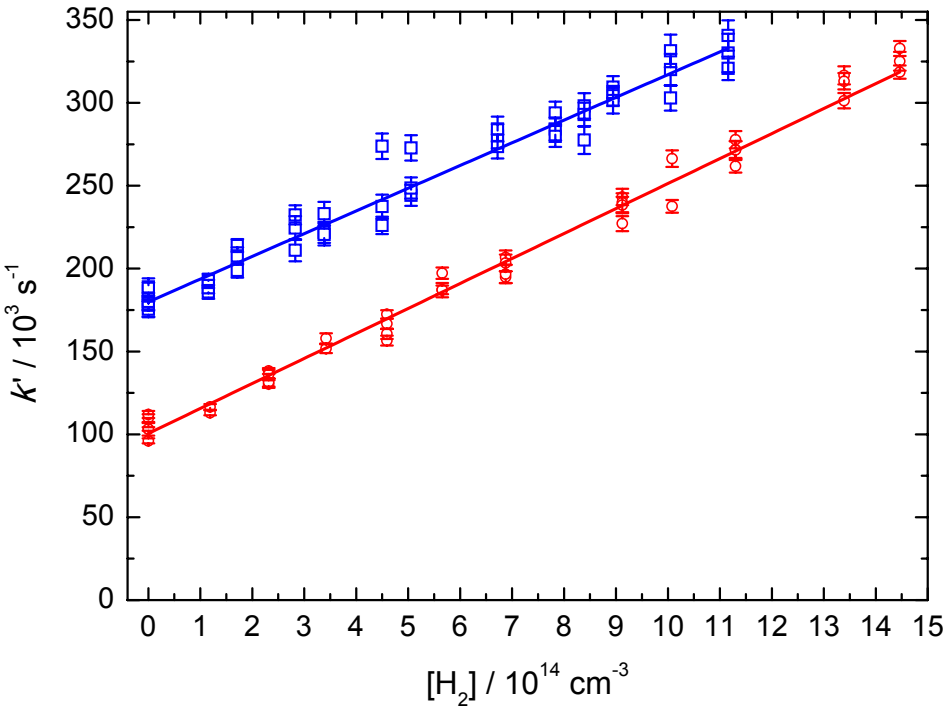

Figure 2 Second-order plots for the $O(^1D) + H_2$ reaction. (red open circles) 296 K experiments; (blue open squares) 50 K experiments. Error bars represent the statistical uncertainties on the

pseudo-first-order rate constants derived from single-exponential fits to the individual O(^{1}D) decays. Second-order rate constants were determined by weighted fits (solid red and blue lines) to the data.

Non-linear least squares fits to the data (weighted by the uncertainties of the exponential fits to each O(^{1}D) decay) yielded the second-order rate constants from the slopes.

The measured second-order rate constants for the O(^{1}D) + H_2 reaction are shown in Figure 3 as a function of temperature alongside the present RPMD rate constants and previous experimental and theoretical studies.

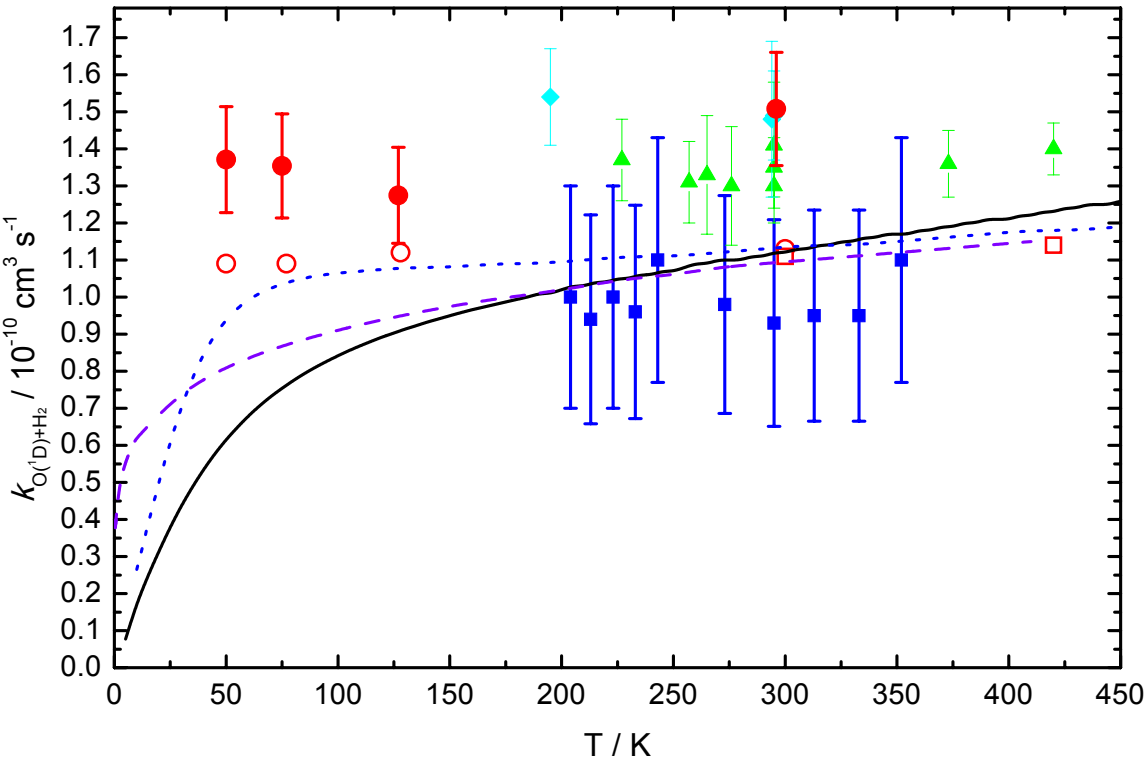

Figure 3 Temperature dependence of the second-order rate constants for the O(^{1}D) + H_2 reaction. Experimental values: (Blue solid squares) Davidson et al.[4]; (light blue solid diamonds) Blitz et al.[14]; (green solid triangles) Vranckx et al.[15]; (Red solid circles) this work. Theoretical

values: (sold black line) Lin & Guo[37]; (dashed blue line) Statistical Quantum Mechanical method (SQM) Rivero-Santamaria et al.[38]; (dashed purple line) Mean Potential Phase Space Theory (MPPST) Rivero-Santamaria et al.[38]; (open red squares) Li et al.[36]; (open red circles) this work RPMD.

The current experimental results are also presented in Table 1 alongside other relevant information. The experimental error bars contain contributions from the statistical uncertainty of second-order fits such as those shown in Figure 2 in addition to an estimated systematic uncertainty of 10 % of the nominal second-order rate constant. In a similar manner to earlier experimental kinetic studies of the title reaction, we find that the measured rate constants display very little variation as a function of temperature with an average value for $k_{O(1D)+H2}$ = (1.38 ± 0.14) × 10^{-10} cm^3 s^{-1}, although this is approximately 15 % larger than the currently recommended value.[1] In common with our previous studies of the $C(^1D) + H_2$ and $C(^1D) + D_2$ reactions, it is expected that the H_2 used in these experiments is non-equilibrated at low temperatures due to inefficient nuclear-spin conversion in the gas-phase between its ortho and para forms. Indeed, this effect results in an order of magnitude increase in the ortho/para ratio for H_2 at 50 K with respect to the equilibrium value, which might lead to a significant deviation of the reaction rate at low temperature. Earlier dynamics experiments investigating the effect of H_2 rotational excitation on the integral cross sections (σ) for the $O(^1D) + H_2$ (J = 1) (ortho) and $O(^1D) + H_2$ (J = 0) (para) reactions determined a ratio σ(J=1)/σ(J=0) = 0.95 ± 0.02 at a collision energy of 5.4 kJ mol^{-1}, indicating only a small reactivity difference towards $O(^1D)$ between these two forms of H_2.[18] Consequently, it is expected that the present kinetic experiments should yield similar rate constants to those conducted at equilibrium. Interestingly however, the reactions of ortho and para H_2 with $O(^1D)$ were seen to lead to quite different quantum state distributions for both forward and backward scattered OH products, indicating potential mechanistic differences for these two processes.

3 Theoretical Methods and Results

The RPMD calculations were performed using the RPMDrate code.[69] The computational procedure is documented in the RPMDrate manual available online (http://rpmdrate.cyi.ac.cy/) and in Suleimanov et al. (2013).[69] RPMD rate theory is well-described in references (36) and (41) and will not be repeated here. In the present calculations, we employed the highly accurate Dobbyn-Knowles potential energy surfaces (PESs).[66] The simulation parameters were taken from the previous studies of insertion type (for the $1^1A'$ surface) and thermally activated (for the $1^1A''$ surface) chemical reactions and are given in Table 2. The main difference between these two sets of parameters is the length of child trajectories in the RPMD transmission coefficient calculations which is ten times longer for the $1^1A''$ state (2 ps versus 0.2 ps for $1^1A'$) due to the long real-time insertion dynamics.[36, 41] The intermediate results are summarized in Figures 4 and 5.

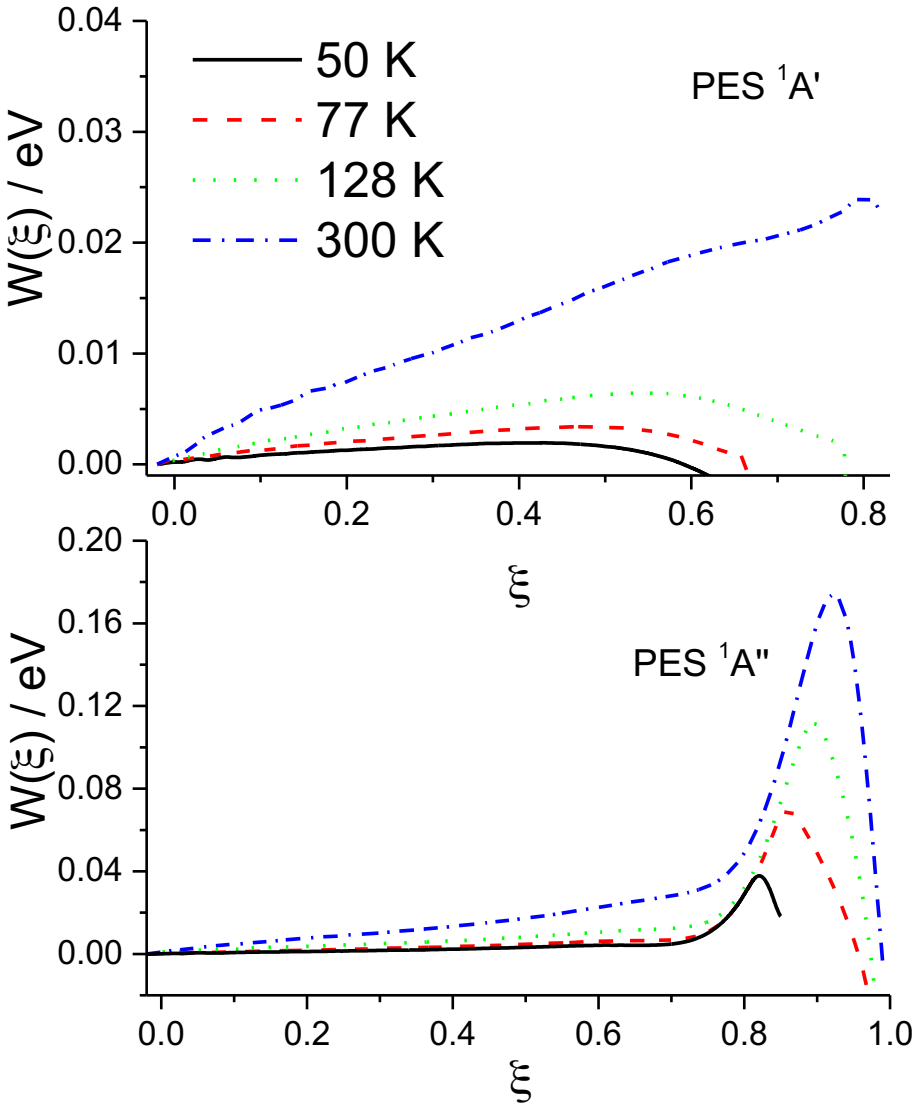

Figure 4 Ring polymer potentials of mean force ($W(\xi)$) along the reaction coordinate for the O(^1D) + H_2 chemical reaction on the ^{1}A' (top panel) and ^{1}A" (bottom panel) PESs at 50, 77, 128 and 300 K.

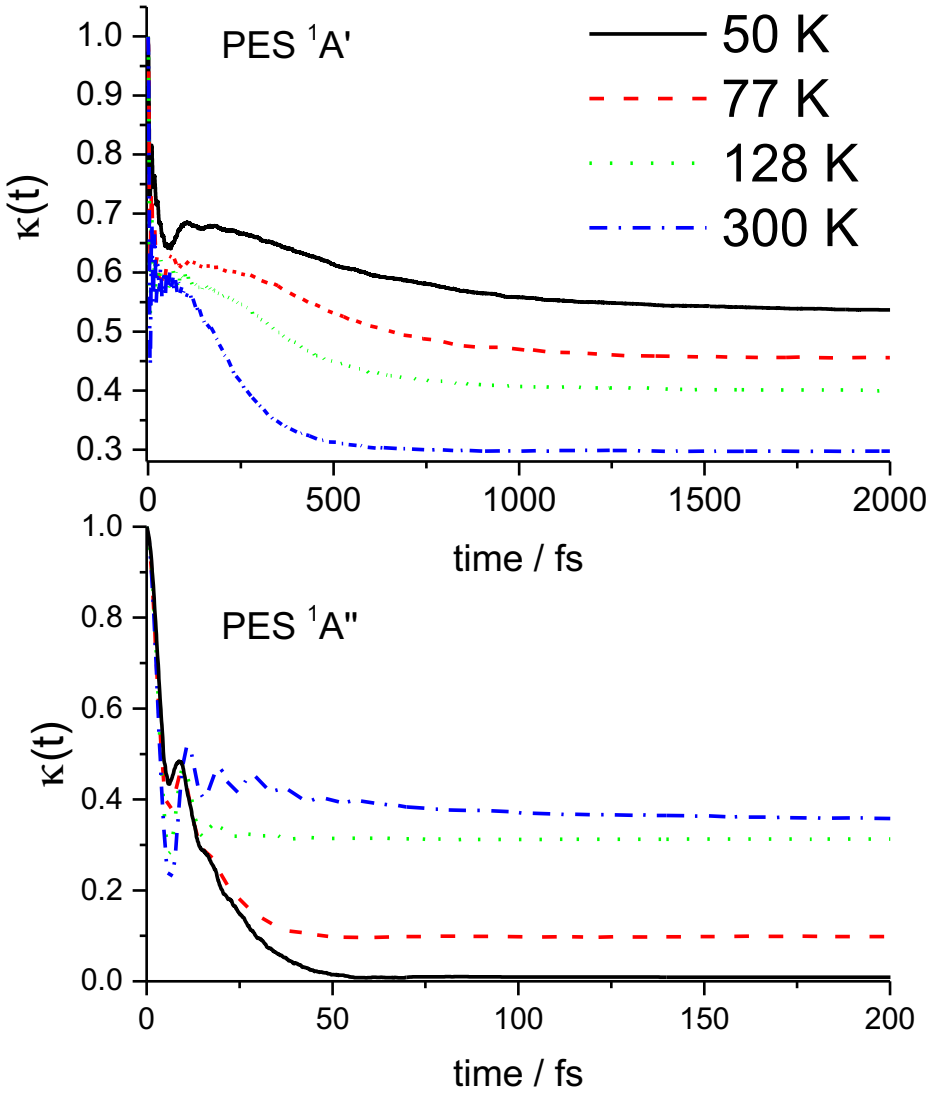

Figure 5 Ring polymer recrossing factors ($\kappa(t)$) along the reaction coordinate for the O(^{1}D) + H_2 chemical reaction on the ^{1}A' (top panel) and ^{1}A" (bottom panel) PESs at 50, 77, 128 and 300 K.

They show that the ring polymer dynamics is quite different on the $1^1A'$ and $1^1A''$ surfaces. As expected, due to the different energy profiles of these PESs, the free energy

counterparts exhibit similar distinctions though the insertion channel ($1^1A'$) also exhibits a free energy barrier (tiny barrier before entering the deep well) due to a decrease in the entropy when damping from unreactive coordinates of the system. The transmission coefficients exhibit a more noticeable distinction with opposite temperature dependences observed for these PESs. These observations are in line with several previous RPMD studies of insertion type and thermally activated chemical reactions.[41]

The final RPMD rate constants are given in Table 3. They show the dominant contribution of the $1^1A'$ ground state to the overall thermal rate constants. The rate constant for the excited state $1^1A''$ rapidly decreases at low temperature due thermal deactivation which is apparently not compensated by quantum tunneling of the light-mass hydrogen atom in this reaction. As a result, the contribution of the $1^1A''$ surface to the overall reactivity decreases to negligible values at the lower temperatures of the present study. We also note that the present result on the $1^1A'$ ground surface at 300 K agrees with the previous RPMD calculations at this temperature.[36]

4 Discussion and Conclusions

In this work, we present a joint experimental and theoretical study of the $O(^1D) + H_2$ gas-phase reaction at low temperatures (300-50 K). Experiments were performed using a continuous supersonic flow reactor coupled with pulsed laser photolysis and pulsed laser induced fluorescence for the production and detection of $O(^1D)$ atoms respectively. Theoretical results were obtained using the recently proposed, though already well-established,[41] ring polymer molecular dynamics (RPMD) method. Calculations were performed for the two lowest adiabatically uncoupled potential energy surfaces (PESs) - the ground $1^1A'$ channel of insertion type and the first excited $1^1A''$ channel which is thermally activated (presenting an energy barrier). The present RPMD calculations confirm the dominant contribution of the barrierless ground $1^1A'$ insertion channel at low temperatures and are in agreement with the experimental

values to within 25 %. However, the RPMD rate constants are seen to decrease below room temperature while the experimental values remain relatively constant. There are several possible explanations for the observed discrepancies. These include the use of non-equilibrated mixtures of H_2 in the present experiments, possible inaccuracies of the underlying PESs which become more important at lower energies, or the adiabatic limit used in the present simulations. Because similar issues appeared in our previous study of the $C(^1D) + H_2$ reaction,[43] we argue that non-adiabatic generalization of RPMD rate theory and the proper treatment of non-adiabatic couplings is extremely important and may improve agreement with the experiment. Indeed, an earlier QM wavepacket investigation[37] of the title reaction adiabatically over the $1^1A'$ and $1^1A''$ states, including a non-adiabatic pathway through coupling between the $1^1A'$ and $2^1A'$ states found that the non-adiabatic channel contributes approximately 10 % to the total rate constant over the entire temperature range. Such an increase in the present RPMD rate constants would clearly bring these values into line with the measured ones (considering the experimental error bars and typical errors of the RPMDrate computational procedure).[41] Several non-adiabatic generalizations of the RPMD theory have been already proposed, e.g., using the mapping approach,[70] such as non-adiabatic RPMD[71] and mapping-variable RPMD.[72] Due to a lack of realistic prototype benchmark systems and comparative analysis with rigorous quantum mechanical results, application of such approaches to the title process will therefore facilitate practical extension of non-adiabatic RPMD rate theory in future.

Acknowledgments

KMH acknowledges support from the French program "Physique et Chimie du Milieu Interstellaire" (PCMI) funded by the Conseil National de la Recherche Scientifique (CNRS) and Centre National d'Etudes Spatiales (CNES). YVS thanks the European Regional Development Fund and the Republic of Cyprus for support through the Research Promotion Foundation (Project Cy-Tera NEA ΥΠΟΔΟΜΗ/ΣΤΡΑΤΗ/0308/31).

References

1. Sander, S. P.; Abbatt J.; Barker J. R.; Burkholder J. B.; Friedl R. R.; Golden D. M.; Huie R. E.; Kolb C. E.; Kurylo M. J.; Moortgat G. K. et al. Chemical Kinetics and Photochemical Data for Use in Atmospheric Studies, Evaluation No. 17. *JPL Publication 10-6, Jet Propulsion Laboratory, Pasadena, 2011* http://jpldataeval.jpl.nasa.gov/. **2011**.
2. Grondin, R.; Loison, J.-C.; Hickson, K. M. Low Temperature Rate Constants for the Reactions of $O(^1D)$ with N_2, O_2, and Ar. *J. Phys. Chem. A* **2016,** *120*, 4838-4844.
3. Meng, Q. Y.; Hickson, K. M.; Shao, K. J.; Loison, J. C.; Zhang, D. H., Theoretical and Experimental Investigations of Rate Coefficients of $O(^1D) + CH_4$ at Low Temperature. *Phys. Chem. Chem. Phys.* **2016,** *18*, 29286-29292.
4. Davidson, J. A.; Schiff, H. I.; Streit, G. E.; McAfee, J. R.; Schmeltekopf, A. L.; Howard, C. J. Temperature Dependence of $O(^1D)$ Rate Constants for Reactions with N_2O, H_2, CH_4, HCl, and NH_3. *J. Chem. Phys.* **1977,** *67*, 5021.
5. Slanger, T. G.; Wood, B. J.; Black, G. Kinetics of $O(^3P)$+CO+M Recombination. *J. Chem. Phys.* **1972,** *57*, 233-238.
6. Kaplan, L. D.; Connes, J.; Connes, P. Carbon Monoxide in Martian Atmosphere. *Astrophys. J.* **1969,** *157*, L187.
7. Barker, E. S. Detection of Molecular-Oxygen in Martian Atmosphere. *Nature* **1972,** *238*, 447-448.
8. Heidner, R. F.; Husain, D. Electronically Excited Oxygen Atoms, $O(2\ ^1D_2)$. A Time-Resolved Study of the Collisional Quenching by the Gases H_2, D_2, CH_4, NO, NO_2, N_2O, and C_3O_2 using Atomic Absorption Spectroscopy in the Vacuum Ultraviolet. *Int. J. Chem. Kinet.* **1973,** *5*, 819-831.
9. Amimoto, S. T.; Force, A. P.; Gulotty, R. G.; Wiesenfeld, J. R. Collisional Deactivation of $O(2\ ^1D_2)$ by the Atmospheric Gases. *J. Chem. Phys.* **1979,** *71*, 3640.
10. Wine, P. H.; Ravishankara, A. R. Kinetics of $O(^1D)$ Interactions with the Atmospheric Gases N_2, N_2O, H_2O, H_2, CO_2, and O_3. *Chem. Phys. Lett.* **1981,** *77*, 103-109.
11. Koppe, S.; Laurent, T.; Naik, P. D.; Volpp, H. R.; Wolfrum, J.; Arusiparpar, T.; Bar, I.; Rosenwaks, S. Absolute Rate Constants and Reactive Cross-Sections for the Reactions of $O(^1D)$ with Molecular Hydrogen and Deuterium. *Chem. Phys. Lett.* **1993,** *214*, 546-552.
12. Matsumi, Y.; Tonokura, K.; Inagaki, Y.; Kawasaki, M., Isotopic Branching Ratios and Translational Energy-Release of H-Atoms and D-Atoms in Reaction of $O(^1D)$ Atoms with Alkanes and Alkyl Chlorides. *J. Phys. Chem.* **1993,** *97*, 6816-6821.
13. Talukdar, R. K.; Ravishankara, A. R. Rate Coefficients for $O(^1D)$+H_2, D_2, HD Reactions and H Atom Yield in $O(^1D)$+HD Reaction. *Chem. Phys. Lett.* **1996,** *253*, 177-183.
14. Blitz, M. A.; Dillon, T. J.; Heard, D. E.; Pilling, M. J.; Trought, I. D. Laser Induced Fluorescence Studies of the Reactions of $O(^1D_2)$ with N_2, O_2, N_2O, CH_4, H_2, CO_2, Ar, Kr and n-C_4H_{10}. *Phys. Chem. Chem. Phys.* **2004,** *6*, 2162.
15. Vranckx, S.; Peeters, J.; Carl, S. Kinetics of $O(^1D) + H_2O$ and $O(^1D) + H_2$: Absolute Rate Coefficients and $O(^3P)$ Yields between 227 and 453 K. *Phys. Chem. Chem. Phys.* **2010,** *12*, 9213-9221.
16. Buss, R. J.; Casavecchia, P.; Hirooka, T.; Sibener, S. J.; Lee, Y. T. Reactive Scattering of $O(^1D)$+H_2. *Chem. Phys. Lett.* **1981,** *82*, 386-391.
17. Alagia, M.; Balucani, N.; Cartechini, L.; Casavecchia, P.; van Kleef, E. H.; Volpi, G. G.; Kuntz, P. J.; Sloan, J. J. Crossed Molecular Beams and Quasiclassical Trajectory Studies of the Reaction $O(^1D)$+H_2 (D_2). *J. Chem. Phys.* **1998,** *108*, 6698-6708.
18. Liu, X.; Wang, C. C.; Harich, S. A.; Yang, X. Effect of a Single Quantum Rotational Excitation on State-to-State Dynamics of the $O(^1D)$+H_2-->OH+H Reaction. *Phys. Rev. Lett.* **2002,** *89*, 133201.

19. Aoiz, F. J.; Banares, L.; Castillo, J. F.; Herrero, V. J.; Martinez-Haya, B.; Honvault, P.; Launay, J. M.; Liu, X.; Lin, J. J.; Harich, S. A. et al. The $O(^1D)+H_2$ Reaction at 56 Mev Collision Energy: A Comparison between Quantum Mechanical, Quasiclassical Trajectory, and Crossed Beam Results. *J. Chem. Phys.* **2002,** *116*, 10692-10703.
20. Gray, S. K.; Balint-Kurti, G. G.; Schatz, G. C.; Lin, J. J.; Liu, X.; Harich, S.; Yang, X. Probing the Effect of the H2 Rotational State in $O(^1D)+H_2 \rightarrow OH+H$: Theoretical Dynamics Including Nonadiabatic Effects and a Crossed Molecular Beam Study. *J. Chem. Phys.* **2000,** *113*, 7330.
21. Liu, X. H.; Lin, J. J.; Harich, S.; Schatz, G. C.; Yang, X. M. A Quantum State-Resolved Insertion Reaction: $O(^1D)+H_2(J=0)$ -> $OH(^2\Pi, \nu, N)+H(^2S)$. *Science* **2000,** *289*, 1536-1538.
22. Liu, Y. F.; Gao, Y. L.; Shi, D. H.; Sun, J. F. Theoretical Study of the Stereodynamics of the Reactions $O(^1D) + H_2$, D_2 and HD. *Chem. Phys.* **2009,** *364*, 46-50.
23. Kuang, D.; Chen, T. Y.; Zhang, W. P.; Zhao, N. J.; Wang, D. J. Effects of Reagent Rotation on Stereodynamics Information of the Reaction $O(^1D)+H_2$ (v=0, J=0-5) -> OH+H: A Theoretical Study. *Bulletin of the Korean Chemical Society* **2010,** *31*, 2841-2848.
24. Lin, S. Y.; Guo, H. Energy Dependence of Differential and Integral Cross Sections for $O(^1D)+H_2$ $\nu_i=0$, $j_i=0$)-->$OH(\nu_f, j_f)$+H Reaction. *J. Chem. Phys.* **2008,** *129*, 124311.
25. Rio, C. M. A.; Brandao, J. Dynamical Studies and Product Analysis of $O(^1D) + H_2/D_2$ reactions. *Mol. Phys.* **2007,** *105*, 359-373.
26. Alexander, M. H.; Rackham, E. J.; Manolopoulos, D. E. Product Multiplet Branching in the $O(^1D)+H_2$ -> $OH(^2\Pi)$+H Reaction. *J. Chem. Phys.* **2004,** *121*, 5221-5235.
27. Hernando, J.; Sayos, R.; Gonzalez, M. A QCT Study of the Microscopic Mechanisms Proceeding via the Ground PES of the $O(^1D)+H_2$ ($X^1\Sigma_g^+$)-> $OH(X^2\Pi)+H(^2S)$ Reaction. *Chem. Phys. Lett.* **2003,** *380*, 123-134.
28. Takayanagi, T. Nonadiabatic Quantum Reactive Scattering Calculations for the $O(^1D)+H_2$, D_2, and HD Reactions on the Lowest Three Potential Energy Surfaces. *J. Chem. Phys.* **2002,** *116*, 2439-2446.
29. Carroll, T. E.; Goldfield, E. M. Coriolis-Coupled Quantum Dynamics for $O(^1D)+H_2$ -> OH+H. *J. Phys. Chem. A* **2001,** *105*, 2251-2256.
30. Honvault, P.; Launay, J. M. A Quantum-Mechanical Study of the Dynamics of the $O(^1D)+H_2$ -> OH+H Insertion Reaction. *J. Chem. Phys.* **2001,** *114*, 1057-1059.
31. Hankel, M.; Balint-Kurti, G. G.; Gray, S. K. Quantum Mechanical Calculation of Product State Distributions for the $O(^1D)+H_2$ -> OH+H Reaction on the Ground Electronic State Surface. *J. Chem. Phys.* **2000,** *113*, 9658-9667.
32. Alexander, A. J.; Aoiz, F. J.; Banares, L.; Brouard, M.; Simons, J. P. Product Rotational Angular Momentum Polarization in the Reaction $O(^1D_2)+H_2$ -> OH+H. *Phys. Chem. Chem. Phys.* **2000,** *2*, 571-580.
33. Gray, S. K.; Goldfield, E. M.; Schatz, G. C.; Balint-Kurti, G. G. Helicity Decoupled Quantum Dynamics and Capture Model Cross Sections and Rate Constants for $O(^1D)+H_2 \rightarrow OH+H$. *Phys. Chem. Chem. Phys.* **1999,** *1*, 1141-1148.
34. Gray, S. K.; Petrongolo, C.; Drukker, K.; Schatz, G. C. Quantum Wave Packet Study of Nonadiabatic Effects in $O(^1D)+H_2$ -> OH+H. *J. Phys. Chem. A* **1999,** *103*, 9448-9459.
35. Drukker, K.; Schatz, G. C. Quantum Scattering Study of Electronic Coriolis and Nonadiabatic Coupling Effects in $O(^1D)+H_2$ -> OH+H. *J. Chem. Phys.* **1999,** *111*, 2451-2463.
36. Li, Y.; Suleimanov, Y. V.; Guo, H. Ring-Polymer Molecular Dynamics Rate Coefficient Calculations for Insertion Reactions: $X + H_2$ --> $HX + H$ (X = N, O). *J. Phys. Chem. Lett.* **2014,** *5*, 700-705.
37. Lin, S. Y.; Guo, H. Adiabatic and Nonadiabatic State-to-State Quantum Dynamics for $O(^1D) + H_2(X^1\Sigma_g^+, \nu_i = j_i = 0)$ --> $OH(X^2\Pi, \nu_f, j_f) + H(^2S)$ Reaction. *J. Phys. Chem. A* **2009,** *113*, 4285-4293.

38. Rivero-Santamaria, A.; Gonzalez-Martinez, M. L.; Gonzalez-Lezana, T.; Rubayo-Soneira, J.; Bonnet, L.; Larregaray, P. The $O(^1D) + H_2$ ($X^1\Sigma_g^+$, v, j) --> $OH(X^2\Pi$, v', j') + H((2)S) Reaction at Low Collision Energy: When a Simple Statistical Description of the Dynamics Works. *Phys. Chem. Chem. Phys.* **2011,** *13*, 8136-8139.
39. Rackham, E. J.; Huarte-Larranaga, F.; Manolopoulos, D. E. Coupled-Channel Statistical Theory of the $N(^2D)+H_2$ and $O(^1D)+H_2$ Insertion Reactions. *Chem. Phys. Lett.* **2001,** *343*, 356-364.
40. Aoiz, F. J.; Banares, L.; Castillo, J. F.; Brouard, M.; Denzer, W.; Vallance, C.; Honvault, P.; Launay, J. M.; Dobbyn, A. J.; Knowles, P. J. Insertion and Abstraction Pathways in the Reaction $O(^1D_2) + H_2$-->OH+H. *Phys. Rev. Lett.* **2001,** *86*, 1729-1732.
41. Suleimanov, Y. V.; Aoiz, F. J.; Guo, H. Chemical Reaction Rate Coefficients from Ring Polymer Molecular Dynamics: Theory and Practical Applications. *J. Phys. Chem. A* **2016,** *120*, 8488-8502.
42. Suleimanov, Y. V.; Kong, W. J.; Guo, H.; Green, W. H. Ring-Polymer Molecular Dynamics: Rate Coefficient Calculations for Energetically Symmetric (near Thermoneutral) Insertion Reactions $(X + H_2)$ --> HX + H ($X = C(^1D), S(^1D)$). *J. Chem. Phys.* **2014,** *141*, 244103.
43. Hickson, K. M.; Loison, J.-C.; Guo, H.; Suleimanov, Y. V. Ring-Polymer Molecular Dynamics for the Prediction of Low-Temperature Rates: An Investigation of the $C(^1D) + H_2$ Reaction. *J. Phys. Chem. Lett.* **2015,** *6*, 4194-4199.
44. Hickson, K. M.; Suleimanov, Y. V. An Experimental and Theoretical Investigation of the $C(^1D) + D_2$ Reaction. *Phys. Chem. Chem. Phys.* **2017**, *19*, 480-486.
45. Rampino, S.; Suleimanov, Y. V. Thermal Rate Coefficients for the Astrochemical Process $C + CH^+ \rightarrow C_2^+ + H$ by Ring Polymer Molecular Dynamics. *J. Phys. Chem. A* **2016,** *120*, 9887-9893.
46. Collepardo-Guevara, R.; Suleimanov, Y. V.; Manolopoulos, D. E. Bimolecular Reaction Rates from Ring Polymer Molecular Dynamics. *J. Chem. Phys.* **2009,** *130*, 14.
47. Suleimanov, Y. V.; Collepardo-Guevara, R.; Manolopoulos, D. E. Bimolecular Reaction Rates from Ring Polymer Molecular Dynamics: Application to $H+CH_4$ -> H_2+CH_3. *J. Chem. Phys.* **2011,** *134*, 10.
48. Collepardo-Guevara, R.; Suleimanov, Y. V.; Manolopoulos, D. E. Bimolecular Reaction Rates from Ring Polymer Molecular Dynamics (Vol 130, 174713, 2009). *J. Chem. Phys.* **2010,** *133*, 2.
49. Li, Y. L.; Suleimanov, Y. V.; Yang, M. H.; Green, W. H.; Guo, H. Ring Polymer Molecular Dynamics Calculations of Thermal Rate Constants for the $O(^3P) + CH_4$ -> OH + CH_3 Reaction: Contributions of Quantum Effects. *J. Phys. Chem. Lett.* **2013,** *4*, 48-52.
50. Li, Y. L.; Suleimanov, Y. V.; Green, W. H.; Guo, H. Quantum Rate Coefficients and Kinetic Isotope Effect for the Reaction $Cl + CH_4$ -> $HCl + CH_3$ from Ring Polymer Molecular Dynamics. *J. Phys. Chem. A* **2014,** *118*, 1989-1996.
51. de Tudela, R. P.; Aoiz, F. J.; Suleimanov, Y. V.; Manolopoulos, D. E. Chemical Reaction Rates from Ring Polymer Molecular Dynamics: Zero Point Energy Conservation in $Mu+H_2$ -> MuH+H. *J. Phys. Chem. Lett.* **2012,** *3*, 493-497.
52. Suleimanov, Y. V.; de Tudela, R. P.; Jambrina, P. G.; Castillo, J. F.; Saez-Rabanos, V.; Manolopoulos, D. E.; Aoiz, F. J. A Ring Polymer Molecular Dynamics Study of the Isotopologues of the $H + H_2$ Reaction. *Phys. Chem. Chem. Phys.* **2013,** *15*, 3655-3665.
53. Allen, J. W.; Green, W. H.; Li, Y. L.; Guo, H.; Suleimanov, Y. V. Communication: Full Dimensional Quantum Rate Coefficients and Kinetic Isotope Effects from Ring Polymer Molecular Dynamics for a Seven-Atom Reaction $OH + CH_4$ -> $CH_3 + H_2O$. *J. Chem. Phys.* **2013,** *138*, 4.
54. Gonzalez-Lavado, E.; Corchado, J. C.; Suleimanov, Y. V.; Green, W. H.; Espinosa-Garcia, J. Theoretical Kinetics Study of the $O(^3P) + CH_4/CD_4$ Hydrogen Abstraction Reaction:

The Role of Anharmonicity, Recrossing Effects, and Quantum Mechanical Tunneling. *J. Phys. Chem. A* **2014,** *118*, 3243-3252.
55. Perez de Tudela, R.; Suleimanov, Y. V.; Richardson, J. O.; Saez Rabanos, V.; Green, W. H.; Aoiz, F. J. Stress Test for Quantum Dynamics Approximations: Deep Tunneling in the Muonium Exchange Reaction D + HMu --> DMu + H. *J. Phys. Chem. Lett.* **2014,** *5*, 4219-4224.
56. Li, Y. L.; Suleimanov, Y. V.; Li, J.; Green, W. H.; Guo, H. Rate Coefficients and Kinetic Isotope Effects of the X + CH_4 -> CH_3 + HX (X = H, D, Mu) Reactions from Ring Polymer Molecular Dynamics. *J. Chem. Phys.* **2013,** *138*, 9.
57. Suleimanov, Y. V.; Espinosa-Garcia, J. Recrossing and Tunneling in the Kinetics Study of the OH + CH_4 -> H_2O + CH_3 Reaction. *J. Phys. Chem. B* **2016,** *120*, 1418-1428.
58. Arseneau, D. J.; Fleming, D. G.; Li, Y. L.; Li, J.; Suleimanov, Y. V.; Guo, H. Rate Coefficient for the ^{4}He Mu + CH_4 Reaction at 500 K: Comparison between Theory and Experiment. *J. Phys. Chem. B* **2016,** *120*, 1641-1648.
59. Meng, Q. Y.; Chen, J.; Zhang, D. H. Communication: Rate Coefficients of the H + CH_4 -> H_2 + CH_3 Reaction from Ring Polymer Molecular Dynamics on a Highly Accurate Potential Energy Surface. *J. Chem. Phys.* **2015,** *143*, 5.
60. Meng, Q. Y.; Chen, J.; Zhang, D. H. Ring Polymer Molecular Dynamics Fast Computation of Rate Coefficients on Accurate Potential Energy Surfaces in Local Configuration Space: Application to the Abstraction of Hydrogen from Methane. *J. Chem. Phys.* **2016,** *144*, 7.
61. Bai, M.; Lu, D.; Li, Y.; Li, J. Ring-Polymer Molecular Dynamical Calculations for the F + HCl → HF + Cl Reaction on the Ground 1^2A' Potential Energy Surface. *Phys. Chem. Chem. Phys.* **2016,** *18*, 32031-32041.
62. de Tudela, R. P.; Suleimanov, Y. V.; Menendez, M.; Castillo, J. F.; Aoiz, F. J. A Ring Polymer Molecular Dynamics Study of the Cl + O_3 Reaction. *Phys. Chem. Chem. Phys.* **2014,** *16*, 2920-2927.
63. Espinosa-Garcia, J.; Fernandez-Ramos, A.; Suleimanov, Y. V.; Corchado, J. C. Theoretical Kinetics Study of the F(^{2}P) + NH_3 Hydrogen Abstraction Reaction. *J. Phys. Chem. A* **2014,** *118*, 554-560.
64. Zuo, J. X.; Li, Y. L.; Guo, H.; Xie, D. Q. Rate Coefficients of the HCl + OH -> Cl + H_2O Reaction from Ring Polymer Molecular Dynamics. *J. Phys. Chem. A* **2016,** *120*, 3433-3440.
65. Ho, T.-S.; Hollebeek, T.; Rabitz, H.; Harding, L. B.; Schatz, G. C. A Global H_2O Potential Energy Surface for the Reaction O(^{1}D)+H_2→OH+H. *J. Chem. Phys.* **1996,** *105*, 10472.
66. Dobbyn, A. J.; Knowles, P. J. A Comparative Study of Methods for Describing Non-Adiabatic Coupling: Diabatic Representation of the $^1\Sigma^+/^1\Pi$ HOH and HHO Conical Intersections. *Mol. Phys.* **1997,** *91*, 1107-1123.
67. Daugey, N.; Caubet, P.; Bergeat, A.; Costes, M.; Hickson, K. M. Reaction Kinetics to Low Temperatures. Dicarbon + Acetylene, Methylacetylene, Allene and Propene from 77 ≤ T ≤ 296 K. *Phys. Chem. Chem. Phys.* **2008,** *10*, 729-737.
68. Hickson, K. M.; Loison, J.-C.; Lique, F.; Kłos, J. An Experimental and Theoretical Investigation of the C(^{1}D) + N_2 → C(^{3}P) + N_2 Quenching Reaction at Low Temperature. *J. Phys. Chem. A* **2016,** *120*, 2504-2513.
69. Suleimanov, Y. V.; Allen, J. W.; Green, W. H. RPMDrate: Bimolecular Chemical Reaction Rates from Ring Polymer Molecular Dynamics. *Comput. Phys. Commun.* **2013,** *184*, 833-840.
70. Ananth, N.; Miller III, T. F. Exact quantum statistics for electronically nonadiabatic systems using continuous path variables. *J. Chem. Phys.* **2010**, *133*, 234103.

71. Richardson, J. O.; Thoss, M. Communication: Nonadiabatic ring-polymer molecular dynamics. *J. Chem. Phys.* **2013**, *139*, 031102.
72. Ananth, N. Mapping variable ring polymer molecular dynamics: A path-integral based method for nonadiabatic processes. *J. Chem. Phys.* **2013**, *139*, 124102.

Table 1 Measured second-order rate constants for the $O(^1D) + H_2$ reaction.

T / K	N^b	$[H_2]$ / 10^{14} cm^{-3}	$k_{O(1D)+H2}$ / cm^3 s^{-1}
296	40	0 - 14.5	$(1.5 \pm 0.2)^c \times 10^{-10}$
127 ± 2[a]	42	0 - 9.8	$(1.3 \pm 0.1) \times 10^{-10}$
75 ± 2	41	0 - 8.0	$(1.4 \pm 0.1) \times 10^{-10}$
50 ± 1	42	0 - 11.2	$(1.4 \pm 0.1) \times 10^{-10}$

[a]Uncertainties on the calculated temperatures represent the statistical (1σ) errors obtained from Pitot tube measurements of the impact pressure. [b]Number of individual measurements. [c]Uncertainties on the measured rate constants represent the combined statistical and systematic errors as explained in the text.

Table 2 Input parameters for the RPMDrate calculations on the $O(^1D) + H_2$. The explanation of the format of the input file can be found in the RPMDrate code manual (see http://rpmdrate.cyi.ac.cy).

Parameter	Potential Energy Surface		Explanation
	$^1A'$	$^1A''$	
Command line parameters			
Temp	300 128 77 50		Temperature (K)
N_{beads}	128 (300 K); 196 (128 K); 256 (77 K); 296 (50 K)		Number of Beads
Dividing surface parameters			
R_∞	15 a_0	15 a_0	Dividing surface parameter (distance)
N_{bond}	1	1	Number of forming and breaking bonds
$N_{channel}$	2	2	Number of equivalent product channels
Thermostat	'Andersen'	'Andersen'	Thermostat option
Biased sampling parameters			
$N_{windows}$	111	111	Number of Windows
$\xi 1$	-0.05	-0.05	Center of the first window
$d\xi$	0.01	0.01	Window spacing step
ξN	1.05	1.05 (0.85 at 50 K)	Center of the last window
dt	0.0001	0.0001	Time step (ps)
ki	2.72	2.72	Umbrella force constant ((T/K) eV)
$N_{trajectory}$	200	200	Number of trajectories
$t_{equilibration}$	20	20	Equilibration period (ps)
$t_{sampling}$	100	100	Sampling period in each trajectory (ps)
N_i	2×10^8	2×10^8	Total number of sampling points
Potential of mean force calculation			
ξ_0	0.00	0.00	Start of umbrella integration
ξ_t	0.570 (300 K) 0.549 (128 K)* 0.494 (77 K)* 0.430 (50 K)*	0.922 (300 K)* 0.896 (128 K)* 0.860 (77 K)* 0.819 (50 K)*	End of umbrella integration
N_{bins}	5000	5000	Number of bins
Recrossing factor calculation			
dt	0.0001	0.0001	Time step (ps)
$t_{equilibration}$	20	20	Equilibration period (ps) in the constrained (parent) trajectory
$N_{totalchild}$	200000	200000	Total number of unconstrained (child) trajectories
$t_{childsampling}$	2	2	Sampling increment along the parent trajectory (ps)
N_{child}	100	100	Number of child trajectories per one initially constrained configuration
t_{child}	2	0.2	Length of child trajectories (ps)

*Detected automatically by RPMDrate;

Table 3 The results of RPMD calculations for the $O(^1D) + H_2$ reaction over the $^1A'$ and $^1A''$ PESs at 50, 77, 128 and 300 K: ring polymer transmission coefficient ($\kappa_{plateau}$) and final RPMD rate coefficients (k_{RPMD}). All rate coefficients are given in cm^3s^{-1}.

T (K)	$\kappa_{plateau}$	k_{RPMD} no correction (with correction)[a]
	PES $1^1A'$	
300	0.297[b]	5.64×10^{-10} (1.13×10^{-10})
128	0.400	5.62×10^{-10} (1.12×10^{-10})
77	0.456	5.42×10^{-10} (1.08×10^{-10})
50	0.537	5.46×10^{-10} (1.09×10^{-10})
	PES $1^1A''$	
300	0.331	1.54×10^{-12} (3.08×10^{-13})
128	0.324	3.48×10^{-14} (6.96×10^{-15})
77	0.098	5.41×10^{-15} (1.08×10^{-15})
50	0.011	2.66×10^{-15}(5.32×10^{-16})

[a] corrected by electronic partition functions $Q_{el} = 5$. [b] calculated at not optimal position of the dividing surface ($\xi = 0.57$) in order to compare with the previous results from Ref. (36) and to verify the independence of RPMD rates from ξ.

TOC Entry

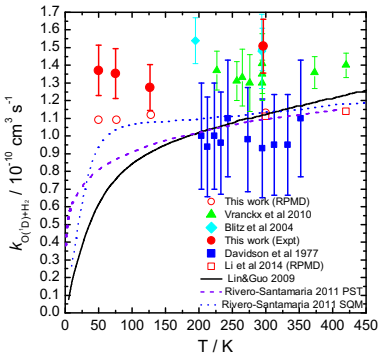
$k_{O(^1D)+H_2}$ / 10^{-10} cm^3 s^{-1}
T / K
This work (RPMD)
Vranckx et al 2010
Blitz et al 2004
This work (Expt)
Davidson et al 1977
Li et al 2014 (RPMD)
Lin&Guo 2009
Rivero-Santamaria 2011 PST
Rivero-Santamaria 2011 SQM